Linear viscoelasticity of concentrated hard-sphere dispersions

1994 J. Phys.: Condens. Matter 6 6423

(http://iopscience.iop.org/0953-8984/6/32/005)

J. Phys.: Condens. Matter 6 (1994) 6423–6436. Printed in the UK

Linear viscoelasticity of concentrated hard-sphere dispersions

D M Heyes and P J Mitchell

Department of Chemistry, University of Surrey, Guildford GU2 5XH, UK

Received 10 January 1994, in final form 20 May 1994

Abstract. The viscoelastic behaviour of model near hard-sphere continuous potential r^{-36} dispersions have been determined using Brownian dynamics simulations in a hydrodynamics-free approximation. Two methods were used to obtain the real and imaginary components of the complex shear viscosity, η' and η'', respectively: first, calculating a time correlation function under no-shear conditions using a Green–Kubo formula; secondly applying finite-strain amplitude oscillatory shear cycles in the linear response limit to the contents of the BD cell. We find that the normalized stress autocorrelation function can be approximated very well by a two-parameter stretched exponential over the complete volume fraction range. The state dependence of the derived spectrum of relaxation times is determined. As for experimental systems the complex viscosity scales with a 'longest' relaxation time, in dimensionless form, $D_0\tau_l/a^2$, where a is the radius of the particle and D_0 is the self-diffusion coefficient in the zero-density limit. Also in the intermediate-frequency regime $40 < a^2\omega/D_0 < 400$ we find that both the real and imaginary parts of the complex shear viscosity decay as $\sim \omega^{-1/2}$ in agreement with experiment and theory. The Newtonian viscosities obtained using $\eta'(\omega \to 0)$ agree well with the predictions of the Krieger–Dougherty equations. The product of the Newtonian viscosity and the long-time self-diffusion coefficient increases linearly with volume fraction for most of the fluid range.

1. Introduction

The dynamical properties of systems of interacting near hard-sphere colloidal dispersions have been studied extensively over recent years. The viscoelastic response to an oscillatory flow field is characterized by a complex viscosity composed of real and imaginary parts, η' the in-phase and η'' the out-of-phase response, respectively. There is a viscoelastic response at all volume fractions (except in the Einstein limit), which is increasingly dominated by the many-body relaxation of the colloidal particles as the volume fraction increases. The linear viscoelasticity for stabilized dispersions has been measured experimentally by van der Werff *et al* (1989) in the volume fraction range $0.10 < \phi < 0.60$. They discovered an inverse-square-root dependence of both $\eta' - \eta'(\infty)$ (where $\eta'(\infty)$ is the infinite-oscillation-frequency viscosity) and η'' in an intermediate-frequency regime $\sim 40 < a^2\omega/D_0 < 400$ where a is the radius of the particle and D_0 is the self-diffusion coefficient in the zero-density limit. Cichocki and Felderhof (1991, 1993) and de Schepper (1993) derived analytic expressions for the complex viscosities, using an approximate form for the spectrum of relaxation times of the stress relaxation function, which also lead to dynamic viscosities with a high-frequency $\sim \omega^{-1/2}$ limiting behaviour. Here we report the results of Brownian dynamics simulations of model stabilized dispersions that explore the viscoelastic response. We calculate the *linear* dynamic viscosities by two methods. In the first method, the

0953-8984/94/326423+14$19.50

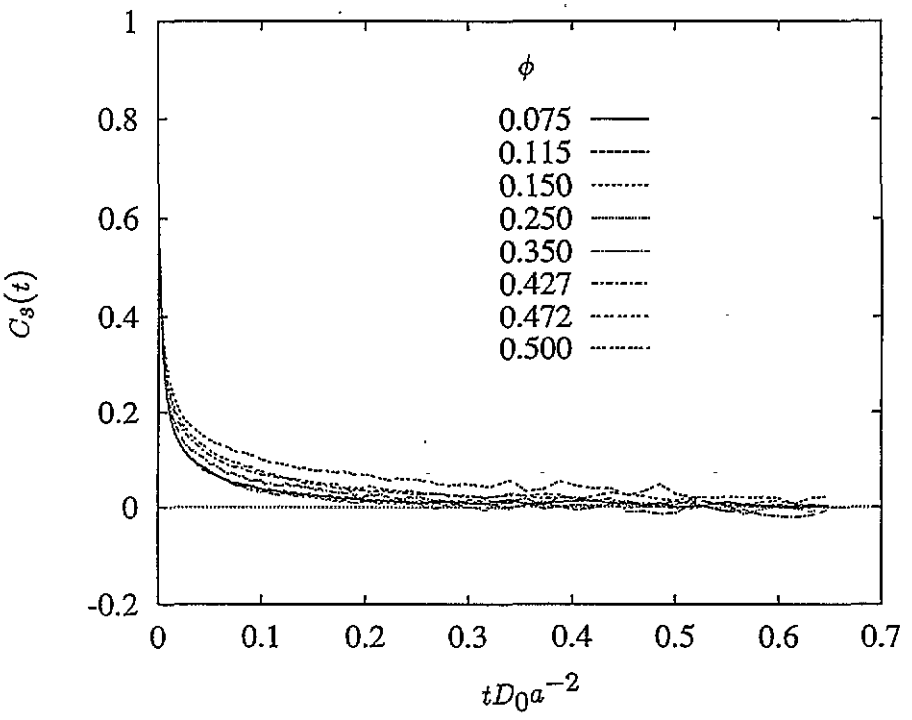

Figure 1. The stress relaxation autocorrelation function, $C_s(t)$ for the state points of volume fraction given on the figure. $N = 108$ in each case.

temporal evolution of the shear stress fluctuations *in an unsheared sample* are used to calculate a time correlation function, $C_s(t)$, which is numerically identical to the shear stress relaxation function measured in linear step-strain rheology experiments. The Fourier transform of $C_s(t)$ gives the complex moduli and shear viscosities. The advantage of this approach is that because no shear rate or strain is applied to the system, then the response function extracted from the simulation is guaranteed to be in the linear response regime, which can be difficult to establish by the direct application of a shear strain profile to the system.

The second route to the dynamic viscosities is to use non-equilibrium BD. The model dispersion is subjected to a homogeneous oscillating shear flow field with a $\exp(-i\omega t)$ time variation, in analogous fashion to the operation of oscillatory shear rheometers where the liquid is excited into a non-equilibrium state by an externally applied wall-driven strain field.

2. Brownian dynamics simulations

The Brownian dynamics method is the same as has been used in previous work, consisting of N coupled irreversible equations of motion for the colloidal particles of mass m at particle positions r_i $(1 \leqslant i \leqslant N)$

$$m\ddot{\boldsymbol{r}}_i = \boldsymbol{F}_i + \boldsymbol{R}_i - \xi\dot{\boldsymbol{r}}_i \tag{1}$$

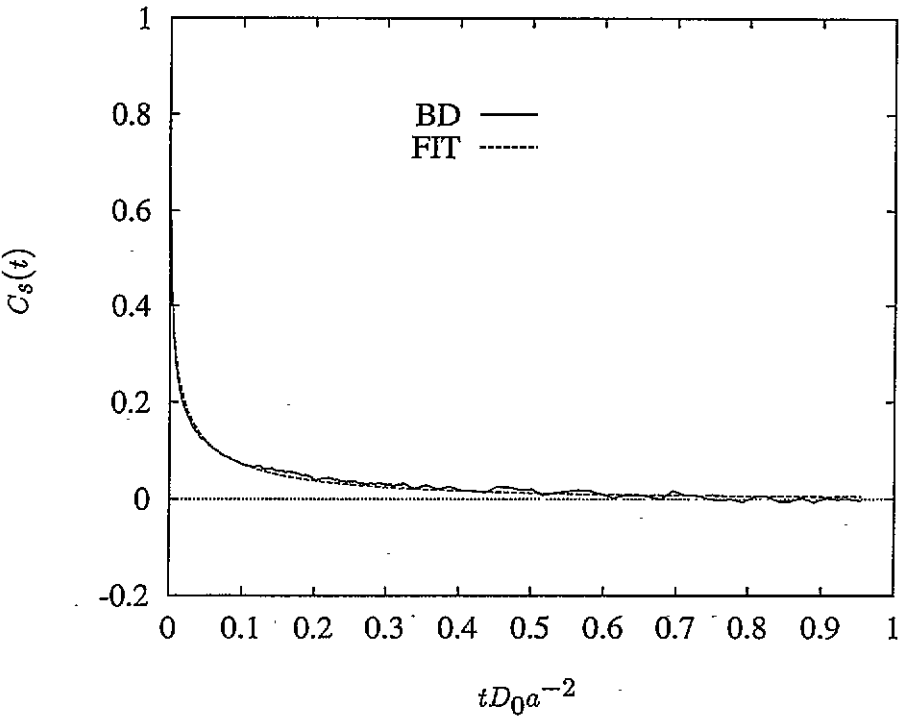

Figure 2. The normalized stress relaxation autocorrelation function from simulation and compared with the stretched exponential least-squares fit for the state $\phi = 0.450$, $\beta = 0.315$ and $\tau' = 0.00465$.

where $\boldsymbol{F}$ is an effective interaction force calculated from

$$\boldsymbol{F}_i = -\nabla \sum_{j \neq i} V(|\boldsymbol{r}_i - \boldsymbol{r}_j|) \tag{2}$$

where V is an effective chemical interaction between colloidal particles, i and j, which is assumed to be pair-wise additive. $\boldsymbol{R}$ is the Langevin random force and ξ is the friction coefficient. The timescale for momentum relaxation of the colloidal particle, called the Brownian relaxation time, is $\tau_B = m\xi^{-1} = m/3\pi\sigma\eta_s$, where η_s is the viscosity of the suspending medium. An integration of equation (1) in the creeping flow limit gives an algorithm that evolves the assembly of particles through time and space

$$r_x(t+h) = r_x(t) + (F_x(t) + R_x(t,h))h/\xi + \dot{\gamma}(t)hr_y. \tag{3}$$

The last term in equation (3) allows for the inclusion of a time-dependent linear shear-flow field in the suspending medium. In the present model we have omitted many-body hydrodynamics, to discover the predictive ability of a simple 'reference' model of a colloidal system. The colloidal particles interact through an inverse power potential where σ is the equivalent hard-core diameter of the model colloid molecule and r is the separation between the centres of two model particles.

$$V(r) = \epsilon(\sigma/r)^n. \tag{4}$$

We set $\epsilon = k_BT$ and $n = 36$. This interaction would represent a stabilized colloidal particle and is sufficiently hard to be equivalent to a hard-sphere system for many purposes. The

reduced number density of particles, $\rho = N\sigma^3/V$ and the solids volume fraction, $\phi = \pi\rho/6$.

The frequency ω is made dimensionless in this work by multiplying by a characteristic structural relaxation time, τ_r, which is the time it takes a colloidal particle at infinite dilution to diffuse a distance $\sqrt{6}a$ where $a = \sigma/2$

$$\tau_r = 3\pi\sigma^3\eta_s/4k_BT = a^2/D_0. \tag{5}$$

For colloidal particles of diameter in excess of 0.1 μm, $\tau_B \ll \tau_r$, so we can choose a time step h such that $\tau_B \ll h \ll \tau_r$. The time step in the simulation, h, is chosen with $h = \delta_m^2/2D_0$, where δ_m is the standard deviation of the random displacement. The value of δ_m was chosen as large as possible within the bounds of algorithm stability and accuracy (determined empirically from a series of simulations and checking for variations in D_L/D_0 and U/N, for example). We typically chose the value $\delta_m = 0.009\sigma$. A hard-sphere Brownian dynamics algorithm proposed by Cichocki and Hinsen (1990) revealed a strong sensitivity of the self-diffusion coefficient to time step. In their algorithm, trial moves were rejected if they resulted in particle overlap. The sensitivity of the self-diffusion coefficient to the magnitude of the time step using this procedure is a pathological feature of their algorithm because the effective size of the particle depends on the root mean square Brownian displacement, so the effective volume fraction at constant particle number density is dependent on the time step. In these inverse power model colloidal systems there is no such configuration rejection criterion, which results in a much smaller dependence of the system's properties on the magnitude of the time step. Comparisons between long-time diffusion coefficients of the inverse power potential for $n = 36$ and the hard-sphere data of Cichocki and Hinsen (1992) reveal excellent agreement, in some sense vindicating both techniques. For example, the values of D_L/D_0 are 0.82 and 0.29 at volume fractions of 0.1 and 0.4, respectively, from both techniques.

For the inverse power potentials considered here, the interaction energy, pressure and mechanical properties are trivially related. The average interaction energy per particle is

$$u = \frac{1}{2N}\sum_{i=1}^{N}\sum_{j\neq i}^{N}\langle V_{ij}(r_{ij})\rangle \tag{6}$$

where $r_{ij} = r_i - r_j$. Then the osmotic pressure is given by

$$P = n\rho\langle u\rangle/3 \tag{7}$$

and the infinite-frequency shear rigidity modulus in the zero-strain-amplitude limit, $G_\infty = G'(\omega \to \infty)$, is given by

$$G_\infty = (n^2 - 3n)\rho\langle u\rangle/15 \tag{8}$$

making use of the formula of Zwanzig and Mountain (1965). Similarly for the infinite-frequency bulk rigidity modulus in the zero-strain-amplitude limit, $K_\infty = K'(\omega \to \infty)$, is given by

$$K_\infty = (n^2 + 3n)\rho\langle u\rangle/9. \tag{9}$$

The stress tensor, $\underline{\sigma}$, is in terms of the microscopic details

$$\underline{\sigma} = \rho k_BT\mathbf{I} + \frac{\rho}{N}\sum_{i=1}^{N-1}\sum_{j=i+1}^{N}(\underline{r}_{ij}\underline{r}_{ij}/r_{ij})V'_{ij} \tag{10}$$

where $\mathbf{I}$ is the identity matrix. The first term in equation (10) is the kinetic contribution to the stress, and the second term is the contribution to the stress from the direct interactions

between the colloidal particles. It does not include the solvent-colloidal particle or solvent-mediated hydrodynamic forces between the colloidal particles. The stress in this free-draining level of approximation is treated at a pair-wise additive level. For a more realistic representation including hydrodynamic interactions, the relationship between particle stress and macroscopic properties is much more complex (see for example Felderhof (1987) and Brady (1993)). On the timescale of the motion of the Brownian particle, they have reached thermal equilibrium due to the large number of collisions with the solvent molecules. The magnitude of the kinetic component of the stress is negligible and much smaller than the potential term (equation (10)). Also as we are mainly interested in the off-diagonal elements of the stress tensor, we do not need to include it because the kinetic contribution to the stress is a diagonal matrix on the rheological timescale. Therefore we do not need to consider the kinetic component and have omitted it in our calculations of the stress tensor.

We also compute the long-time, D_L self-diffusion coefficient from the 'local' slope of the mean square displacement with time curve, i.e.

$$D(t) = \frac{1}{6}\frac{\mathrm{d}\langle \Delta r(t)^2 \rangle}{\mathrm{d}t} \tag{11}$$

where $D_L = D(t \to \infty)$ and $\Delta r(t) = r_i(t) - r_i(0)$ for arbitrary particle of index i. The use of this definition of a time-dependent self-diffusion coefficient was discussed by Cichocki and Hinsen (1992). This approach converges more rapidly to the asymptotic limit than $\langle \Delta r(t)^2 \rangle / 6t$. The slopes were taken for times in excess of $2.5a^2/D_0$.

2.1. *Time correlation function*

A linear response expansion of the position Langevin equation used in this work (e.g. Hess and Klein (1983)) leads to a Green–Kubo expression for the linear shear viscosity in terms of the shear stress time autocorrelation function, $C_s(t)$, defined as

$$C_s(t) = \frac{N}{\rho k_B T}\langle \sigma_{xy}(0)\sigma_{xy}(t) \rangle \tag{12}$$

where $\langle \cdots \rangle$ indicates an average over time origins in equation (12). This method was first used by Levesque *et al* (1973) who applied it to molecular liquids. The infinite-frequency linear shear modulus is given by $G_\infty = C_s(0)$. In an unsheared system, the stress fluctuations of all the off-diagonal elements of the stress tensor are equivalent. Therefore, we improved the statistics of $C_s(t)$ by considering σ_{xy}, σ_{xz}, and σ_{yz} separately in equation (12), and then averaging the three at the end of the simulation. (The stress tensor is symmetric so $\sigma_{\alpha\beta} = \sigma_{\beta\alpha}$.) The function, $C_s(t)$, is exactly the same function as the stress relaxation function derived from step-in-strain experiments taken in the linear strain limit. The time correlation functions have to extend typically for $\sim 20\,000$ time steps to ensure decay of the function to zero. In order to reduce the computer memory requirements, the correlation function was constructed in a piece-wise fashion from three separate correlation functions with time origins started every (and with a resolution of) 1, 10 and 100 time steps. These three correlation functions extended for progressively longer in time, and non-overlapping pieces were merged for the purpose of subsequent analysis and presentation. The number of entries in the histogram used to calculate the time correlation function decreases as time increases. Nevertheless the statistics is reasonable for the $\sim 500\,000$ time steps covered for each production simulation.

The present BD model (described in greater detail by Heyes and Melrose (1993) and Melrose and Heyes (1993)) only incorporates the thermodynamic interactions between the colloidal particles and ignores the many-body hydrodynamic solvent-mediated forces. A

measure of the contribution of many-body hydrodynamics to the total viscosity is given by the experimental value of the viscosity in the second Newtonian plateau, η_∞, which is entirely hydrodynamic in origin. If we assume that the hydrodynamic contribution to the viscosity is equal to η_∞ at *all* shear rates, then the Green–Kubo formula in the present model gives the difference between the Newtonian viscosity η_0 (the zero-shear-rate limit) and η_∞. The Newtonian viscosity, η_0, is then related to $C_s(t)$ through

$$\eta_0 = \eta_\infty + \int_0^\infty C_s(t)\,\mathrm{d}t \tag{13}$$

where we need to take a value for η_∞ from another source. The same argument applies in the case of oscillation, in that we can only monitor deviations from $\eta'(\infty)$, the real part of the infinite-frequency viscosity.

It is convenient to render the colloidal liquid's viscosity dimensionless by dividing by the viscosity of the suspending medium. This leads to so-called *relative* viscosities, $\eta_{r0} = \eta_0/\eta_s$ and $\eta_{r\infty} = \eta_\infty/\eta_s$. The complex dynamic viscosity is

$$\eta^*(\omega) = \eta'(\omega) + \mathrm{i}\eta''(\omega). \tag{14}$$

The dynamic shear modulus, $G^*(\omega) = G'(\omega) + \mathrm{i}G''(\omega)$ where $G'(\omega) = \omega\eta''(\omega)$ and $G''(\omega) = \omega\eta'(\omega)$. We have

$$\eta'(\omega) = \eta'(\infty) + \Im(\mathrm{i}\int_0^\infty C_s(t)\mathrm{e}^{-\mathrm{i}\omega t}\mathrm{d}t) \tag{15}$$

and

$$\eta''(\omega) = \Re(\mathrm{i}\int_0^\infty C_s(t)\mathrm{e}^{-\mathrm{i}\omega t}\mathrm{d}t) \tag{16}$$

where $\eta'(\infty) = \eta_\infty$. $C_s(t)$ can be represented by a superposition of exponential relaxation functions

$$C_s(t) = G_\infty \int_0^\infty p(\tau)\mathrm{e}^{-t/\tau}\mathrm{d}\tau \tag{17}$$

with the normalization condition $\int_0^\infty p(\tau) = 1$. Then

$$\eta^*(\omega) = \eta'(\infty) + G_\infty \int_0^\infty \frac{\tau p(\tau)\,\mathrm{d}\tau}{(1+\omega\tau\mathrm{i})} = \eta'(\infty) + G_\infty \int_{-\infty}^\infty \frac{\tau H(\tau)\,\mathrm{d}\ln(\tau)}{(1+\omega\tau\mathrm{i})} \tag{18}$$

where $H(\tau) = \tau p(\tau)$.

A non-equilibrium BD technique which can be used to compute the complex viscosities in both the linear and non-linear response regimes is described in the next section.

2.2. *Applied oscillatory shear*

The contents of the BD cell are sheared homogeneously with a time-dependent strain over n cycles

$$\gamma(t) = \gamma_0 \cos\omega t \tag{19}$$

where γ_0 is the strain amplitude. The analytic expressions for the dynamic viscosities are

$$\eta' = \frac{1}{n\pi\gamma_0}\int_0^{2n\pi/\omega} \sigma_{xy}(t')\,\mathrm{d}t'\sin(\omega t') \tag{20}$$

and

$$\eta'' = \frac{1}{n\pi\gamma_0}\int_0^{2n\pi/\omega} \sigma_{xy}(t')\,\mathrm{d}t'\cos(\omega t'). \tag{21}$$

The number of cycles in a simulation of a specified number of time steps and oscillatory frequency was adjusted to be a whole number by scaling down the time step. The number of cycles varied with the value of $\omega\tau_r$. The number was adjusted empirically to produce reasonable statistics for the average quantities. For example, for $\omega\tau_r > 100$ we chose $n = 200$ and for $\omega\tau_r < 0.1$ we used $n = 10$. Limitations on the availability of computer time necessitated a smaller number of cycles at low frequency, as each cycle takes an increasing number of time steps as the frequency decreases. Therefore, the statistical uncertainty of the cycle averages was larger as frequency was lowered.

In the following section we use the time correlation method and direct application of a shear flow to explore the linear viscoelasicity of these model colloidal liquids over a wide volume fraction range.

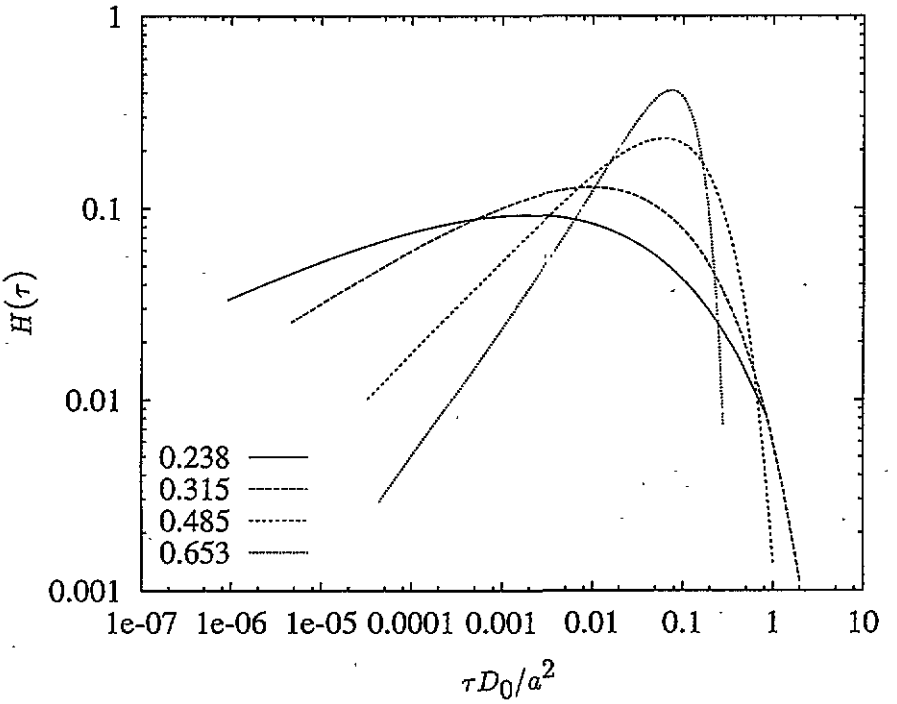

Figure 3. Plot of the stretched exponential relaxation time spectrum distribution function for the values: (a) $\beta = 0.238$ and $\tau' = 0.000907$, (b) $\beta = 0.315$ and $\tau' = 0.00465$, (c) $\beta = 0.485$ and $\tau' = 0.0306$, (d) $\beta = 0.653$ and $\tau' = 0.0414$.

3. Results and discussion

A series of equilibrium Brownian dynamics simulations was carried out at a range of volume fractions using $N = 108, 256$ and 500. Simulation details are given in table 1. The first three D_L/D_0 in table 1, for $\phi = 0.075, 0.115$ and 0.150 fit well to $D_L/D_0 = 1 - a\phi$ with the coefficient $a = 1.7 \pm 0.2$ close to the prediction of the hypothetical case of hard spheres without hydrodynamic interactions $a = 2.0$ (Ackerson and Fleishman 1982).

Above a volume fraction of $\phi \sim 0.4$ there is an increasing system size dependence for

Table 1. Thermodynamic, mechanical and Newtonian transport coefficients from Green–Kubo formulae. KD is the value of $\eta_{t0}-\eta_{t\infty}$ from the Krieger–Dougherty formulae (Russel *et al* 1989). The mean square force in the α-cartesian direction is $\langle F_\alpha^2\rangle$. The thermodynamic and mechanical quantities are accurate to $\sim 1\%$, while the viscosity has a larger error of ~ 2–3%. Only the interaction components of the thermodynamic and mechanical quantities are given. t_{sim} is the length of the production simulation. Key: (a) $n = 6$ in equation (4); (b) $n = 12$ in equation (4); otherwise $n = 36$.

N	ϕ	t_{sim}/τ_t	u	$\langle F_\alpha^2\rangle$	D_L/D_0	G_∞	$\eta_{t0}-\eta_{t\infty}$	KD
108	0.075	455	0.0322	27.98	0.880	0.365	0.016	0.038
108	0.115	143	0.0563	48.97	0.799	0.979	0.044	0.073
108	0.150	444	0.0819	71.35	0.749	1.857	0.069	0.115
108	0.250	113	0.1892	166.3	0.581	7.155	0.295	0.366
108	0.350	63	0.3893	346.3	0.402	20.61	0.995	1.17
256	0.400	330	0.5443	485.7	0.291	32.93	1.90	2.26
108	0.427	397	0.6572	590.1	0.253	42.45	3.05	3.34
500	0.427	170	0.6599	592.3	0.230	42.62	2.95	—
500	0.450	207	0.7750	700.0	0.193	52.75	3.97	4.79
108	0.472	153	0.8939	811.7	0.154	63.82	7.10	7.00
256	0.472	151	0.8945	811.8	0.150	63.86	7.05	—
500[a]	0.472	159	4.0706	78.84	0.431	4.40	0.61	—
500[b]	0.472	175	2.4609	218.91	0.254	15.97	2.54	—
500	0.472	217	0.9016	819.1	0.157	64.37	> 5.4	—
256	0.490	182	1.0169	927.4	0.124	75.37	10.9	9.83
500	0.490	243	1.0232	934.4	0.115	75.84	7.9	—
108	0.500	122	1.0763	984.0	0.110	81.40	12.2	12.1
108	0.527	133	1.0579	955.6	0.047	84.33	> 250	22.4
256	0.527	113	1.1293	1026.0	0.029	90.02	> 56	—
500	0.527	146	1.3327	1233.6	0.053	106.23	> 31	—

the calculated properties, as expected because configurational phase space becomes more structured with increasing ϕ. Only those configurations consistent with a finite periodic system are allowed, which produces an increasingly more unrepresentative average with increasing ϕ. Generally the internal energy (and other derived properties) and the viscosities decrease with increasing N. The self-diffusion coefficients increase with N. The system size dependence is an important factor which must be considered for volume fractions in excess of 0.40, and that is why we performed simulations on increasingly large numbers of particles as the volume fraction increases.

Table 1 reveals that the 108 to 500 values of $\eta_{t0}-\eta_{t\infty}$ at $\phi = 0.427$ are 3.05 to 2.95 respectively, compared with 7.10 to > 5.4 at $\phi = 0.472$. There is a small N dependence at $\phi = 0.427$ but a more significant effect at $\phi = 0.472$. Where uncertainties exist we state this (e.g. in table 1). However, we only extensively analyse and discuss the behaviour of the state points (typically $\phi = 0.427$ and 0.472 and below) for which we are confident that we are close enough to the thermodynamic limit not to influence our conclusions. Figure 1 shows that the $C_s(t)$ become more long-lived with increasing ϕ. The shape of these curves can be represented very well by a so-called 'fractional' or 'stretched' exponential (except at very short times $t/\tau_t < 0.2\times 10^{-2}$ where it underestimates the simulation $C_s(t)$)

$$C(t) = G_\infty \exp(-(t/\tau')^\beta). \tag{22}$$

An example of the fit is given in figure 2. In table 2 we summarize the values of τ' and β for the different systems. We also give in the table the mean relaxation time $\tau = \tau'\Gamma(1/\beta)/\beta$

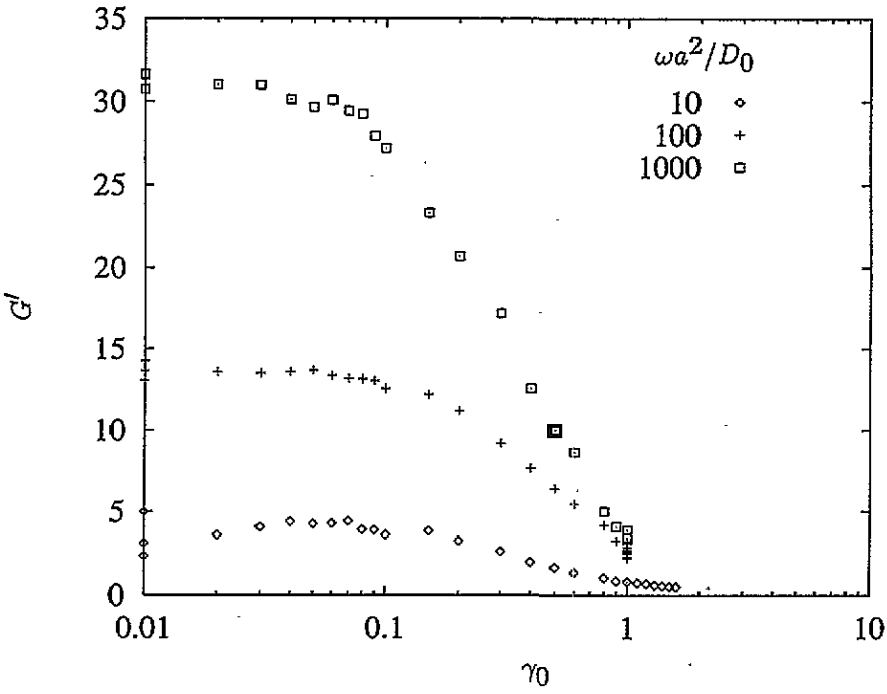

Figure 4. The strain amplitude γ_0 dependence of the storage modulus of a $N = 108$ and $\phi = 0.427$ system at the frequencies $\omega\tau_r = 10$ $\omega\tau_r = 100$ and $\omega\tau_r = 1000$.

for the normalized function

$$\tau = \int_0^\infty \exp(-(t'/\tau')^\beta)\, dt'. \tag{23}$$

The simulations show that the mean relaxation time increases with volume fraction in agreement with the experimental data on sterically stabilized silica particles by van der Werff *et al* (1989).

In the $\phi \to 0$ limit the stress relaxation function appears to be relatively insensitive to the value of ϕ. In this region the parameters have values $\beta = 0.37 \pm 0.01$ and $\tau' = 0.0035 \pm 0.0001$ for $\phi < 0.25$. There is a gradual decrease in the value of β and increase in τ' with increasing volume fraction. The functional form of equation (22) can be written alternatively in the form of equation (17). The distributions of relaxation times $p(\tau)$ or equivalently $H(\tau)$ for several representative choices of β and τ' are presented in figure 3 using the numerical procedure developed by Lindsey and Patterson (1980) specifically for the stretched exponential (see also Montroll and Bendler (1984)). The figure shows that the stretched exponential produces a relaxation time distribution function with a relatively sharp cut-off at the high-τ end, which gets sharper as $\beta \to 1$ (being a δ function for $\beta = 1$). There is a slower decay of $H(\tau)$ in the $\tau \to 0$ limit. The spectrum of relaxation times becomes broader as β decreases with increasing ϕ. Also data for three different softnesses of interaction are specified by variable n values in equation (4). The figure reveals that as the interaction becomes softer (n decreases) then the relaxation function more closely approaches a single exponential (i.e. $\beta \to 0$). If each of these relaxation times is identified

Table 2. The parameters of the stretched exponential least-squares fit to the simulation $C_s(t)$ from equation (22). The mean relaxation time is defined in equation (23). Key: (a) $n = 6$ in equation (4); (b) $n = 12$ in equation (4); otherwise $n = 36$.

N	ϕ	β	τ'/τ_r	τ/τ_r
108	0.075	0.362	0.003 47	0.0156
108	0.115	0.360	0.003 40	0.0155
108	0.150	0.381	0.003 60	0.0137
108	0.250	0.384	0.003 70	0.0138
108	0.350	0.355	0.004 04	0.0193
256	0.400	0.331	0.003 72	0.0228
108	0.427	0.320	0.004 20	0.0292
500	0.450	0.315	0.004 65	0.0341
108	0.472	0.287	0.003 69	0.0398
256	0.472	0.283	0.004 09	0.0465
500[a]	0.472	0.653	0.0414	0.0563
500[b]	0.472	0.485	0.0306	0.0648
500	0.472	0.309	0.004 72	0.0373
256	0.490	0.278	0.004 45	0.0540
500	0.490	0.306	0.006 04	0.0493
108	0.500	0.269	0.004 40	0.0603
256	0.527	0.111	0.000 344	0.281
500	0.527	0.239	0.005 71	0.116

with a particlular microscopic mechanism for stress release, then this trend indicates that there are many more significant dynamical processes, with a wide distribution of relaxation times, involved in stress relaxation at the higher volume fractions. The rapid decrease in $C_s(t)$ occurs in the time domain of the transition between the short- and long-time diffusion coefficients.

In table 1 we give the integrated shear viscosity from equation (13). The states at $\phi = 0.472$ and above manifest an N dependence with the $N = 500$ being the largest number of particles considered. Over the complete volume fraction range the following analytic expressions fit the experimental relative viscosity data of near hard-sphere dispersions (summarized in the Krieger–Dougherty expressions (Russel 1989)) quite well. The expressions are

$$\eta_{r0} = (1 - \phi/0.63)^{-2} \tag{24}$$

and

$$\eta_{r\infty} = (1 - \phi/0.71)^{-2}. \tag{25}$$

The Krieger–Dougherty expression for $\eta_{r0} - \eta_{r\infty}$, gives values that are statistically very close to the simulation results (obtained by numerical integration of the time correlation functions) which is quite remarkable as the model has no many-body hydrodynamics in the equations of motion. This indicates that at these high volume fractions, the simple Langevin dynamics embodied in the computer algorithm used here reproduces well the rheology of the real systems. We now consider the oscillatory shear simulations carried out using the non-equilibrium BD method. We are interested in the linear response region here, so it is important to determine the maximum strain amplitude that can be used (which will depend on frequency) to retain a good approximation within the linear response regime. In figure 4 we explore the strain amplitude dependence of the storage modulus, G', for a $\phi = 0.427$ state. Simulations were carried out over a range of γ_0 between 0.01 and 1.0 at a series

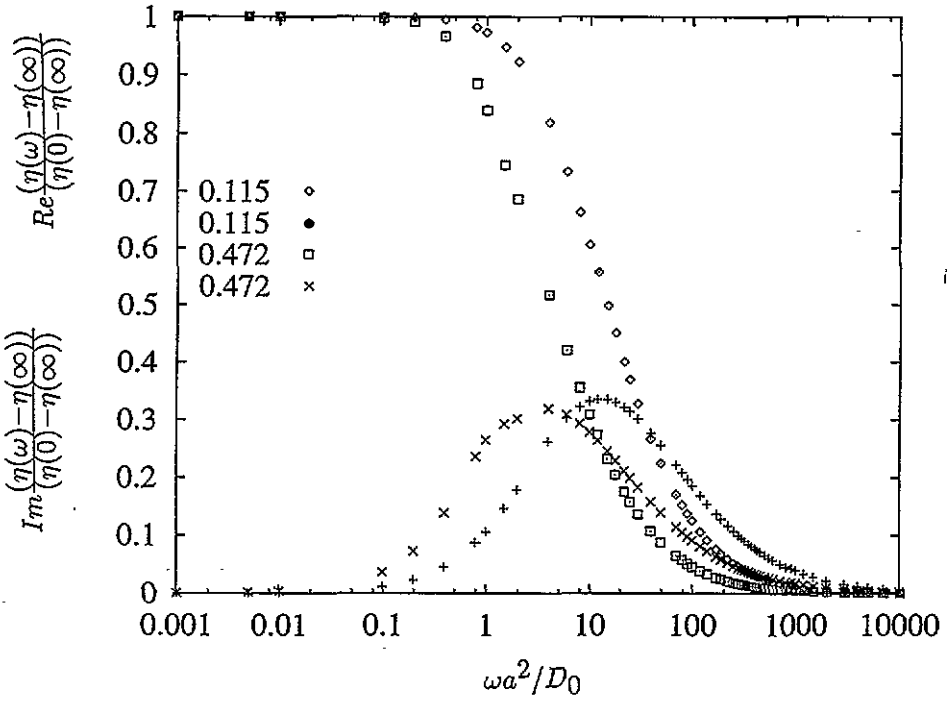

Figure 5. Real (upper curves) and imaginary (lower curves) parts of the relative complex shear viscosity as a function of frequency for the volume fractions $\phi = 0.115$, $N = 108$ and $\phi = 0.472$, $N = 500$.

of fixed frequencies covering the range of interest. The response is linear for $\gamma_0 < 0.1$, showing shear strain 'softening' of the elastic response for higher amplitudes. Values of $\gamma_0 = 0.02$ were chosen for the oscillatory shear simulations to ensure linear response.

The complex viscosities obtained from the stretched exponential fits to the time correlation functions using equation (15) and equation (16), are statistically indistinguishable from those obtained using the direct application of an oscillating shear flow field for $\omega a^2/D_0 < 1000$. At higher frequencies systematic differences appear which arise from the failure of the fit to match the simulation $C_s(t)$ at very short times. The reduced frequency domain of $\omega a^2/D_0 > 1000$ is not, however, of practical interest. The real and imaginary parts of the relative complex viscosity for two widely separated volume fractions are given in figure 5. The η' and η'' shift to lower frequencies as ϕ increases. For $a^2\omega/D_0$ between 4 and 400 figure 6 shows that both the η' and η'' decay as $\omega^{-1/2}$ which can be described by

$$\eta'_r = \eta'_{r\infty} + A'(a^2\omega/D_0)^{-1/2} \tag{26}$$

$$\eta''_r = A''(a^2\omega/D_0)^{-1/2}. \tag{27}$$

This is in agreement with the data of van der Werff *et al* (1989). The dimensionless constants A' and A'' have values 1.8 ± 0.1, 3.6 ± 0.2 and 5.5 ± 0.5 at the volume fractions $\phi = 0.35, 0.427$ and 0.472 respectively. The experimental values at these volume fractions are approximately double in magnitude. For $\phi = 0.35, 0.427$ and 0.472 these parameters have the values 3.5 ± 0.5, 9.0 ± 1.0 and 30 ± 5, which were obtained by interpolating the experimental data on sterically stabilized silica particles from van der Werff *et al* (1989).

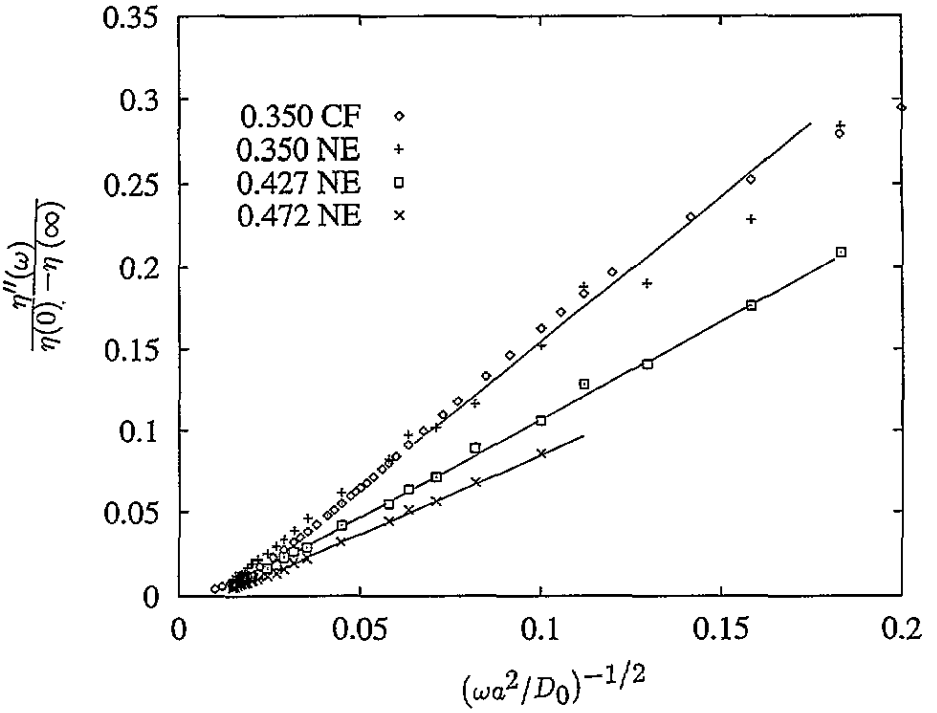

Figure 6. Normalized real part of the relative complex shear viscosity as a function of $(a^2\omega/D_0)^{-1/2}$ for $\phi = 0.350$, 0.427 and 0.472. CF denotes Fourier transformation of the correlation function and NE denotes the non-equilibrium BD method.

The mode coupling theory of Cichocki and Felderhof (1991) gives values of A'' equal to 0.22, 0.33 and 0.40, for these state points. van der Werff *et al* (1989) also show that the complex viscosity scales with a reduced frequency, $\omega a^2\tau_1/D_0$, where τ_1 is the 'longest' relaxation time in their fit to the data. If we use the van der Werff values for $a^2\tau_1/D_0$ then the present simulation data also scale onto the same curve which is also statistically indistinguishable from their experimental data (see figure 7). The particle size and volume fraction therefore can be incorporated in this dimensionless scaling parameter. The values of $a^2\tau_1/D_0$ are approximately an order of magnitude larger than (but roughly proportional to) the values of $a^2\tau/D_0$ (where τ is defined in equation (23)) which we obtained from our simulations. Cichocki and Felderhof (1992) give a value of the mean relaxation time in the dilute limit $\tau = 2a^2/9D_0$ which is approximately an order of magnitude greater than the values given in table 2. Figure 1 shows that our simulated $C_s(t)$ decay rapidly and that, for a low volume fraction, it is improbable that there is a long-time tail 'hidden' within the noise which could lead to an order of magnitude increase in τ when computed using equation (23). This is especially true for the lowest volume fraction state $\phi = 0.075$ which has a $C_s(t)$ that is statistically indistinguishable from zero for times longer than $t = 0.6a^2/D_0$. Quite clearly there *are* long relaxation times in the time correlation function, but it would appear from our simulations that their amplitudes are rather small, except at high volume fractions near to close packing. This discrepancy does not affect our excellent agreement with the viscoelasticity, in figure 7, however, because this is a function of all the relaxation times in the model, not just the longest.

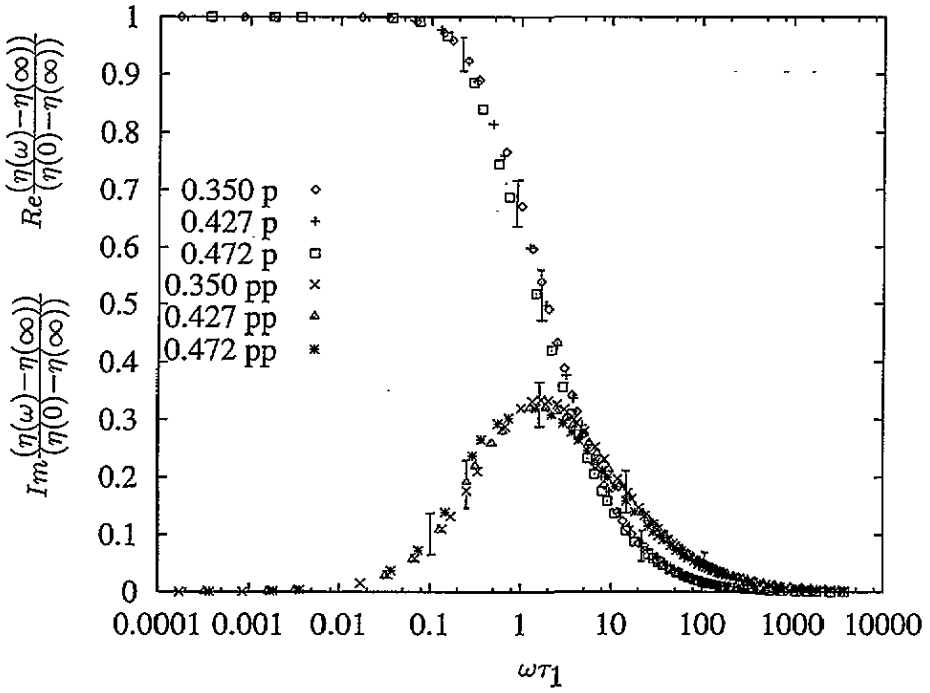

Figure 7. Normalized real and imaginary part of the relative complex shear viscosity as a function of frequency for three volume fractions $\phi = 0.350$, 0.427 and 0.472 versus $\omega\tau_1$, where $D_0\tau_1/a^2 = 0.17$, 0.32 and 0.37 respectively. The 'bars' on the figure represent the limits of the band of experimental points from van der Werff *et al* (1989).

The Stokes–Einstein relationship (applicable in the dilute limit) for this system is $D_L\eta_r(0)/D_0 = 1$. In figure 8 we show that the ratio $D_L\eta_r(0)/D_0$ is essentially linear with volume fraction up to $\phi \sim 0.45$ before levelling off. If it is assumed that the effective particle diameter is volume fraction independent, then this behaviour confirms that the viscosity increases more rapidly with solids fraction than the long-time diffusion coefficient decreases.

4. Conclusions

We have shown that Brownian dynamics computer simulation can be used to investigate the viscoelastic behaviour of model near-hard-sphere colloidal liquids up to volume fractions in excess of 0.50 using two complementary Brownian dynamics procedures (equilibrium and non-equilibrium). The linear stress relaxation function (stress autocorrelation function) is approximated well by a stretched exponential. Despite the absence of many-body hydrodynamics in our model algorithms, the Newtonian and complex shear viscosities give quite good agreement with the experimental values at the same volume fractions.

Acknowledgments

P J M thanks the SERC and ECC International Ltd for a research fellowship (grant number GR/H80644). Computations were carried out on a CONVEX C3 at the University of London

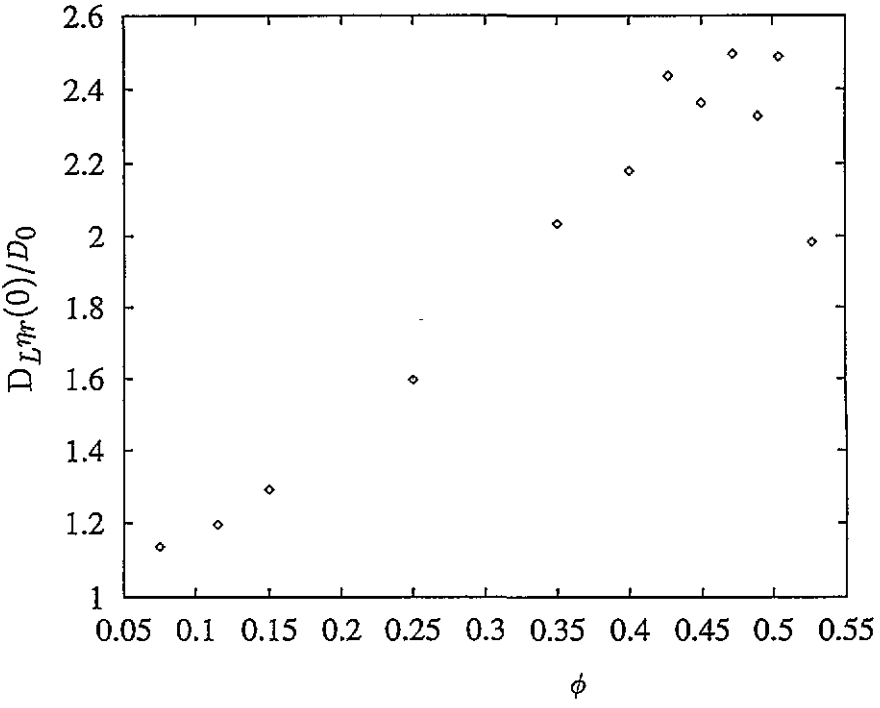

Figure 8. Plot of $D_{L\eta_r}(0)/D_0$ versus volume fraction for the simulation data.

Computer Centre, Personal DECStations and a Silicon Graphics Indigo XZ workstation in the Chemistry Department at the University of Surrey.

References

Ackerson B J and Fleishman L 1982 *J. Chem. Phys.* **76** 2675
Brady J F 1993 *J. Chem. Phys.* **99** 567
Cichocki B and Felderhof B U 1991 *Phys. Rev.* A **43** 5405
—— 1992 *Phys. Rev.* A **46** 7723
—— 1993 *Physica* A **198** 423
Cichocki B and Hinsen K 1990 *Physica* A **166** 473
—— 1992 *Physica* A **187** 133
de Schepper I M, Smorenburg H E and Cohen E G D 1993 *Phys. Rev. Lett.* **70** 2178
Felderhof B U 1987 *Physica* A **147** 203
Gaylor K J, Snook I K, van Megen W and Watts R O 1979 *Chem. Phys.* **43** 233
Hess W and Klein R, 1983 *Adv. Phys.* **32** 173
Heyes D M and Melrose J R 1993 *J. Non-Newtonian Fluid Mech.* **46** 1
Levesque D, Verlet L and Kurkijarvi J 1973 *Phys. Rev.* A **7** 1690
Lindsey C P and Patterson G D 1980 *J. Chem. Phys.* **73** 3348
Löwen H, Hansen J-P and Roux J-N 1991 *Phys. Rev.* A **44** 1169
Melrose J R and Heyes D M 1993 *J. Chem. Phys.* **98** 5873
Montroll E W and Bendler J T 1984 *J. Stat. Phys.* **34** 129
Russel W B, Saville D A and Schowalter W R 1989 *Colloidal Dispersions* (Cambridge: Cambridge University Press) p 466
van der Werff J C, de Kruif C G, Blom C and Mellema J 1989 *Phys. Rev.* A **39** 795
Zwanzig R and Mountain R W 1965 *J. Chem. Phys.* **43** 4464